Molecular Neurobiology (2025) 62:3956–3972
https://doi.org/10.1007/s12035-024-04515-8

ORIGINAL ARTICLE

Vinpocetine Ameliorates Neuronal Injury After Cold-Induced Traumatic Brain Injury in Mice

Hayriye E. Yelkenci[1,2] · Zehra Degirmenci[2] · Halil I. Koc[2] · Sevban Bayirli[2,3] · Saltuk B. Baltaci[2,3] · Serdar Altunay[2,3] · Nevin Oztekin[1] · Mehmet Kocak[4] · Ertugrul Kilic[5] · Mustafa C. Beker[2,5]

Received: 4 November 2023 / Accepted: 15 September 2024 / Published online: 3 October 2024

Abstract

Traumatic brain injury (TBI), also known as intracranial injury, is a common condition with the highest incidence rate among neurodegenerative disorders and poses a significant public health burden. Various methods are used in the treatment of TBI, but the effects of cold-induced traumatic brain injury have not been thoroughly studied. In this context, vinpocetine (VPN), derived from Vinca minor, exhibits notable anti-inflammatory and antioxidant properties. VPN is known for its neuroprotective role and is generally utilized for treating various neurodegenerative disorders. However, the function of VPN after cold-induced TBI needs to be studied in more detail. This study aims to investigate the neuroprotective effects of VPN at varying doses (5 mg/kg or 10 mg/kg) after cold-induced TBI. C57BL/6 mice were sacrificed 2 or 28 days after cold-induced TBI. Results indicate that VPN administration significantly reduces brain infarct volume, brain swelling, blood–brain barrier disruption, and DNA fragmentation in a dose-dependent manner. Additionally, VPN enhances neuronal survival in the ipsilesional cortex. In the long term, VPN treatment (5 mg/kg/day or 10 mg/kg/day, initiated 48 h post-TBI) improved locomotor activity, cell proliferation, neurogenesis, and decreased whole brain atrophy, specifically motor cortex atrophy. We performed liquid chromatography-tandem mass spectrometry (LC–MS/MS) to elucidate the underlying mechanisms to profile proteins and signaling pathways influenced by prolonged VPN treatment post-TBI. Notably, we found that 192 different proteins were significantly altered by VPN treatment, which is a matter of further investigation for the development of therapeutic targets. Our study has shown that VPN may have a neuroprotective role in cold-induced TBI.

Keywords Cold-induced TBI · Neuroprotection · Proteomics · Traumatic brain injury · Vinpocetine

Introduction

Vinpocetine (VPN) is a selective PDE1 inhibitor and a synthetic ethyl-ester derivative of the alkaloid apovincamine from Vinca minor leaves [1]. It has a strong antioxidant capacity, can cross the blood–brain barrier (BBB) and is considered a well-tolerated drug. Recent studies have shown that VPN enhances brain function by supporting the supply of oxygen and glucose [2–4]. VPN enhances intracellular levels of cyclic adenosine 3′,5′-monophosphate (cAMP) and cyclic guanosine 3′,5′-monophosphate (cGMP), activating protein kinase A and protein kinase G, respectively [5, 6]. This effect of VPN also demonstrates anti-inflammatory responses in the neurologic system by inhibiting neuronal voltage-gated sodium channels, such as tetrodotoxin-sensitive voltage-dependent sodium channels, and reducing neuronal influx [1, 7] VPN treatment has been shown to increase intracellular cAMP and cGMP levels, which, in turn, inhibit

✉ Mustafa C. Beker
mustafa.beker@medeniyet.edu.tr; m.caglarbeker@gmail.com

1 Department of Chemistry, Istanbul Technical University, Istanbul, Türkiye

2 Regenerative and Restorative Medical Research Center (REMER), Research Institute for Health Sciences and Technologies (SABITA), Istanbul Medipol University, Istanbul, Türkiye

3 Department of Physiology, School of Medicine, Istanbul Medipol University, Istanbul, Türkiye

4 Department of Biostatistics and Medical Informatics, International School of Medicine, Istanbul Medipol University, Istanbul, Türkiye

5 Department of Physiology, Faculty of Medicine, Istanbul Medeniyet University, Istanbul, Türkiye

neuronal inflammation by reducing the expression of tumor necrosis factor-alpha (TNF-α) and interleukin-1 beta (IL-1β) [8–10]. VPN has been reported to reduce neuroinflammation and improve cerebral blood flow following ischemic stroke [10]. Consequently, VPN has shown effectiveness against cerebral ischemia, memory disorders, and Parkinson's disease [4, 10–12].

Phosphodiesterase 1 (PDE1) subfamily hydrolyzes cAMP and cGMP in a mutually competitive manner [13]. It is well known that second messengers regulate various physiological processes, playing a critical role in neurodevelopment, synaptic plasticity, and axon elongation, such as Wnt or Notch signaling pathways [5, 14, 15]. Because of that, homeostasis of the cellular concentrations of cAMP and cGMP through PDE1 is crucial for regulating intracellular processes and can be an important therapeutic target for the future [16, 17].

Traumatic brain injury (TBI) is caused by an external force that damages the brain's structure, blood vessels, and nerve cells. Millions of individuals are annually affected by TBI, which can result in devastating long-term outcomes [18]. Currently, no treatment effectively improves recovery after TBI, although temporary therapies can be applied acutely following injury. Although VPN treatment may have an effect in different pathophysiological conditions, its role in cold-induced TBI in mice in terms of some parameters, such as proteomic profile, has not yet been revealed. In this study, we investigated the neuroprotective effects of VPN treatment using low dose (5 mg/kg) or high dose (10 mg/kg) administration on infarct volume, brain swelling, blood–brain barrier (BBB) integrity, and disseminated neuronal injury after cold-induced TBI to the cortex. Additionally, we evaluated the long-term effects of VPN (5 mg/kg/day or 10 mg/kg/day) on spontaneous locomotor activity, brain atrophy, cell proliferation, and neurogenesis. Furthermore, we performed liquid chromatography-tandem mass spectrometry (LC–MS/ MS) to determine the protein profile and signaling pathways affected by long-term VPN administration after TBI.

Materials and Methods

Ethics Statement for Animal Experiments

This study has been conducted under the ethics standards of the EU Guidelines on the Care and Use of Laboratory Animals (Directive 2010/63/EU) in agreement with Turkiye Animal Research Ethics Committee local guidelines and legislation. The study has been approved by local government authorities (Istanbul Medipol University, Animal Research Ethics Committee; reference number: 10/01/2022–05). All animals were maintained under a constant 12-h light/dark cycle (lights on at 07:00 daily) with ad libitum access to food and water. Investigators were blinded for experimental groups at all stages of experiments and data analysis.

Experimental Groups

Experiments were performed using adult (8–12 weeks) BALB/c male mice (22–30 g). A total of 72 animals were divided into two main sets. In the first set, vehicle (250 µl saline, containing 10% DMSO), 5 mg/kg VPN (S2110, Selleckchem, USA); dissolved in 250 µl saline, containing 10% DMSO) or 10 mg/kg VPN (dissolved in 250 µl saline containing 10% DMSO) was administered by intraperitoneal injection immediately after cold-induced traumatic brain injury (TBI), and mice were sacrificed 48 h later (Fig. 1A). For the first set, $n = 8$ mice/group were used for brain infarct volume, brain edema, neuronal survival, and DNA fragmentation analysis and $n = 4$ for BBB analysis, which was analyzed by Evans blue staining. In the second set, animals ($n = 12$/ group) received daily oral doses of vehicle, 5 mg/kg VPN, or 10 mg/kg VPN starting from 2 to 28 days post-TBI. To analyze proliferating cells, 100 mg/kg 5′-bromo-2-deoxyuridine (BrdU; B5002; Sigma Aldrich, Missouri, USA) was intraperitoneally injected at 3-day intervals starting from day two until the end of the experiment (Fig. 1B). In addition, an open field test was performed 3 days before and on the 2nd, 7th, 14th, and 28th days after cold-induced TBI to evaluate locomotor activity and exploration behavior.

Cold-Induced Traumatic Brain Injury (TBI) Model

To induce brain injury, animals underwent cold-induced TBI, a commonly utilized animal model that shares essential similarities with trauma in terms of pathophysiological cascades [19]. Briefly, mice were anesthetized with 1.5% isoflurane (30% O_2, reminder N_2O) (AWN-340150–01, Adeka, Turkiye), and rectal temperature was stabilized between 36.5 and 37 °C using a feedback-controlled heating system (K 023152, Harvard, UK). Mice were fixed on a stereotaxic device (WPI Instruments, USA), and its head was secured using ear bars and a tooth bar to immobilize it. The position of the mouse's head was adjusted until the skull landmarks were leveled and aligned properly. After the scalp was sterilized with 70% ethanol, a small incision was made in the scalp, and the connective tissue was removed. Brain injury was performed using a liquid nitrogen-cooled copper probe (tip diameter 1.5 mm), which touched the skull (Bregma 1.0 mm posterior and 1.5 mm lateral). Before each cold-induced TBI, 3 min was allowed for liquid nitrogen to homogenously cool the copper probe. In this way, it was aimed to perform equal damage to each mouse. Then, the probe was directly placed on the skull for 60 s. After 60 s, the probe was carefully removed from the skull. After

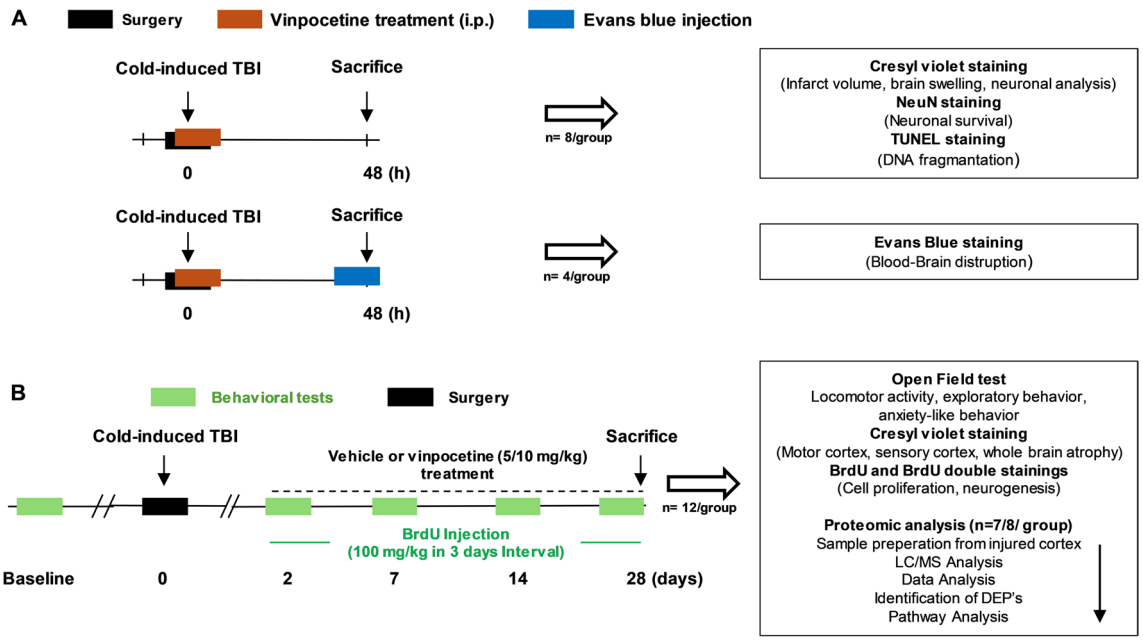

Fig. 1 Schematic representation of the experimental design. **A** To evaluate infarct volume, brain swelling, neuronal injury, neuronal survival, and DNA fragmentation, BALB/c male mice were randomly assigned to vehicle, 5 mg/kg VPN or 10 mg/kg VPN, which was administered by intraperitoneal injection immediately after cold-induced TBI, and mice were sacrificed 48 h later. **B** Mice were submitted to cold-induced TBI followed by 28 days survival. Vehicle or VPN (5 or 10 mg/kg/day) was administered orally 48 h post-TBI. To analyze newly formed cells, 100 mg/kg BrdU was intraperitoneally injected at 3-day intervals starting from 48 h post-TBI

waiting 1 min, the wounds were closed with suture [20]. After that, mice were placed back into their home cages.

Animal Behavioral Test: Open-Field Test

To evaluate spontaneous locomotor activity and exploration behavior, open field test was performed before the animal surgery and 2, 7, 14, and 28 days after the cold-induced TBI. Briefly, the open field maze has a 100-cm diameter, which features a white plastic floor. Encircling the platform is a 35-cm-high side wall constructed from white polypropylene. In each trial, mice were introduced near the arena's periphery and monitored for a duration of 600 s. The arena is divided into three sections, including an outer wall zone (17.7% of diameter, close to the wall), an intermediate transition zone (32.3%ofdiameter), and an inner zone (50%of diameter, the center of the arena). Each mouse was released near the wall and observed for 10 min. Traveled distance in the maze, mobility and immobility time, and time total in the core zone, transition zone, and wall zone were recorded using Anymaze software (Version 4.99; Stoelting, Ireland) [21].

Evaluation of Brain Infarct Volume, Brain Swelling, and Brain Atrophy

Brain infarct volume and brain swelling were calculated from brain sections obtained from mice sacrificed 48 h after cold-induced TBI. Coronal brain sections were obtained at equidistant intervals of 1.5 mm. Following this process, sections were then stained with cresyl violet (C5042; Sigma Aldrich, USA) according to the previously published protocol [19]. Within the sections, the border between injured (I) and non-injured (NI) tissues was delineated using an image analysis software (Image J; National Institute of Health, Maryland, USA). The infarct area was quantified by subtracting the area of the ipsilesional hemisphere non-infarcted (I_{NI}) tissue from that of the contralesional hemisphere (C_H). Infarct volume was calculated by the (C_N—I_{NI}) x distance between injured areas. Brain swelling was determined as the volume difference between the ipsilesional hemisphere (I_H) and the C_H and expressed in cubic millimeters (mm^3).

To assess brain atrophy, sections obtained at 1 mm intervals were subjected to cresyl violet in animals sacrificed 28 days post-cold-induced TBI. The area of atrophy was calculated using ImageJ software, we determined the volumes of both brain hemispheres (I_H and C_H), motor cortex (I_M ipsilesional motor cortex, C_M contralesional motor cortex), or sensory cortex (I_S ipsilesional sensory cortex, C_S contralesional sensory cortex) by outlining respective areas on tissue sections, integrating these areas to calculate volumes, and then expressing the volumes on the lesioned side as a percentage of the corresponding volumes on the contralesional side. By subtracting these volume ratios from 100, we obtained measurements for whole brain atrophy

$(100\text{-}(I_H \times 100)/C_H))$, motor cortex atrophy $(100\text{-}(I_M \times 100)/C_M))$, and sensory cortex atrophy $(100\text{-}(I_S \times 100)/C_S))$.

Analysis of Blood–Brain Barrier (BBB) Integrity

Evans blue staining was performed to examine the BBB permeability after cold-induced TBI. Evans Blue (E2129-10G; Sigma Aldrich) was prepared at 2% (w/v) in normal saline. The dye solution (3 ml/kg) was administered through the tail vein toward blood flow. One hour after injection, the animals were sacrificed by decapitation. The whole brain was removed and cut coronally into 2-mm slices using a brain matrix, with cutting sites corresponding to − 2 mm AP distance from the bregma. Sections were analyzed using an image analysis system (Image J).

Evaluation of Neuronal Survival, Injured Neurons, Non-injured Neurons, and DNA Fragmentation

For the evaluation of neuronal survival, coronal brain sections at the level of the bregma from mice subjected to acute-term cold-induced TBI were fixed with 4% paraformaldehyde (PFA) (158,127-500G; Sigma Aldrich)/0.1 M phosphate-buffered saline (PBS) and incubated at room temperature for 1 h with 0.1 mol/l PBS including 0.3% Triton X-100 (PBS-T)/(A4025-1L; Biomatic, Germany)/10% normal goat serum (NGS) (G9023; Sigma Aldrich). Then, sections were incubated overnight at 4 °C with Alexa Fluor 488-conjugated monoclonal mouse anti-NeuN (Mab377X; Sigma Aldrich). The next day, sections were counterstained with 4′,6-diamidino-2-phenylindole (DAPI) (GE17-0891–01; Sigma Aldrich) and were analyzed using a confocal microscope (LSM800, Carl Zeiss, Jena, Germany). Nine different regions of interest (ROI) in the injured and non-injured cortex, each measuring 62,500 μm^2, were evaluated. Therefore, neuronal survival was calculated by proportioning the mean number of NeuN (+) cells in the injured cortex to the non-injured cortex. To determine injured and non-injured (intact) neurons in the ipsilesional cortex, we used cresyl violet stained sections. Depending on neuronal morphology, shrunken, triangular-shaped, and condensed nuclei were considered damaged neurons.

To evaluate DNA fragmentation, brain sections from the bregma level were fixed with 4% PFA and stained by terminal transferase dUTP nick end labeling (TUNEL) using an in situ cell death detection kit (11,684,795,910; Roche, Switzerland) according to the previously described protocol [22]. Sections were counterstained with DAPI. TUNEL-positive DNA-fragmented cells were counted in 6 ROI in the injured cortex (each of 62,500 μm^2 size) using a confocal laser scanning Zeiss LSM 800 microscope (Carl Zeiss).

Determination of Newly Formed Cells and Neurogenesis

Brain sections at the bregma level from mice subjected to long-term cold-induced TBI were fixed with 4% PFA/0.1 M PBS to analyze newly formed cells and neurogenesis. For antigen retrieval, sections were pretreated with sodium citrate buffer (10 mM sodium citrate (1,064,461,000; Merck, USA), 0.05% tween 20 (P1379; Sigma Aldrich), pH 6.0) rinsed, and immersed for 1 h in 0.1 M PBS containing 0.3% Triton (PBS-T) and 10% NGS. Sections were incubated with Alexa Fluor 488 anti-BrdU Antibody (364,106, Biolegend, USA), used as a cell proliferation marker; Alexa Fluor-555 conjugate anti-NeuN antibody (MAB377A5, Sigma Aldrich), used as a neuronal marker; or Doublecortin (4604, Cell Signaling Technology, USA), used as a migrating neuron marker. The next day, for the sections stained with Doublecortin antibody, secondary antibody incubation was held goat anti-rabbit Alexa Fluor-633 conjugated (A-21071, Invitrogen, USA) for 1 h at room temperature. Then, sections were counterstained with DAPI and were analyzed using a confocal microscope (LSM800, Carl Zeiss). BrdU + cells, BrdU + /NeuN + newborn neurons, and BrdU + /Doublecortin (DCX) + migrating neurons were counted in the 6 ROI in the injured cortex (each of 62,500 μm^2 size).

Sample Preparation for Liquid Chromatography-Tandem Mass Spectrometry (LC–MS/MS)

Brain tissues were dissected from the injured cortex, homogenized in 50 mM ammonium bicarbonate (S2454-200ML, Sigma Aldrich) containing a protease inhibitor cocktail (ab270061, Expedeon, Heidelberg, Germany), and lysed at 95 °C in a protein extraction reagent kit (UPX Universal; Expedeon). The samples were incubated for 1 h at 4 °C after the lysis step. According to the manufacturer's protocol, protein concentrations were determined using a Qubit 3.0 Fluorometer (Q33216, Invitrogen, Life Technologies, USA). Following homogenization, the FASP (Filter Aided Sample Preparation) Protein Digestion Kit (ab270519, Abcam, UK) was used to generate tryptic peptides according to the manufacturer's instructions. A total of 50 µg protein samples were filtered using 6 M urea in a 30-kDa cutoff spin column. After this step, samples were alkylated with 10 mM iodoacetamide in the dark for 20 min at room temperature. Then, samples were incubated overnight with MS grade trypsin protease (ratio 1:100, 90,057, Thermo Fisher Scientific, USA) at 37 °C. The following day, peptides were eluted from the columns

and lyophilized. After the lyophilization process, the peptides were suspended in 0.1% formic acid (1,002,642,510, Merck, USA) and diluted to 100 ng/µl before injecting to the LC–MS/MS system (ACQUITY UPLC M-Class coupled to a SYNAPT G2-Si high-definition mass spectrometer (Waters, MA, USA)).

LC–MS/MS Analysis and Data Processing

LC–MS/MS and protein identification were performed with minor modifications according to previously published protocols [23]. Briefly, samples were loaded onto the ACQUITY UPLC M-Class coupled to a SYNAPT G2-Si high-definition mass spectrometer (Waters). To equilibrate the columns, 97% of the mobile phase (0.1% formic acid in LC–MS grade water) was used, and the column temperature was set to 55 °C. Ninety-minute gradient elution from the trap column ACQUITY UPLC M-Class Symmetry C18 trap column (180 µm × 20 mm; 186,007,496, Waters) to the analytic column (ACQUITY UPLC M-Class HSS T3 Column, 100 Å, 1.8 µm, 75 µm × 250 mm,; 186,007,474, Waters) at 0.400 µL/min flow rate with a gradient from 4 to 40% hypergrade acetonitrile (100,029, Merck) containing 0.1% formic acid (v/v) was used for the peptide separation. Positive ion modes of MS and MS/MS scans with 0.6-s cycle time were performed sequentially. Ten volts were set as low collision energy (CE), and 30 V as high CE. Ion mobility separation (IMS) was used for the ion separation. A wave velocity was ramped from 1000 to 55 m/s over the entire IMS cycle. The release time for mobility trapping was 500 µs, and trap height was set to 15 V. IMS wave delay was 1000 µs for the mobility separation after trap release. All the ions within 50–1900 m/z range were fragmented in resolution mode without any precursor ion preselection. Then, 100 fmol/µL Glu-1-fibrinopeptide B (186,007,091–2, Waters MA, USA) was used for lock mass reference with a 60-s interval to observe the mass stability. Data were performed in Progenesis-QI for proteomics software (Waters) to identify and quantify of the peptides. Vehicle 5 mg/kg VPN and 10 mg VPN treatment samples, which all belong to the ipsilateral area of the brain, were compared together in Progenesis-QI for proteomics. At least two unique peptide sequences identified whole proteins, and then the expression ratio of proteins was calculated.

The pathway analysis was conducted using the Protein ANalysis THrough Evolutionary Relationships (PANTHER; https://www.pantherdb.org/) classification system and The Database for Annotation, Visualization, and Integrated Discovery (DAVID; v2023q4, https://david.ncifcrf.gov/) to utilize Kyoto Encyclopedia of Genes and Genomes (KEGG), REACTOME, and WikiPathways database. A p value threshold of 0.05 was applied during the analysis as a filter. After pathway analysis, enrichment bubble plots were created for the top pathways with enrichment scores, p values, and count values using the online SRplot program (available at https://www.bioinformatics.com.cn/) [24].

Statistics

The data for immunofluorescence and immunohistochemistry experiments are illustrated using raincloud plots generated with jittering, presenting visual representations of the median, interquartile range (IQR) boxes, and 95% confidence intervals (CI) for each quantitative attribute via Jeffrey's Amazing Statistics Program (JASP; Version 0.18.3, Netherlands; available at https://jasp-stats.org) [25]. The normality of the data was assessed using the Shapiro–Wilk test. Subsequently, based on the distribution of the data, the Kruskal–Wallis test was conducted for non-parametric data (DNA fragmentation, whole brain atrophy, motor cortex atrophy, cell proliferation, neurogenesis), while Tukey's multiple comparison test was employed for normally distributed data (infarct volume, brain swelling, BBB leakage, neuronal survival, injured neurons, intact neurons, and sensory cortex atrophy) [26]. Additionally, the Bayesian factor (BF10) was calculated to ascertain the strength of evidence for one-way ANOVA tests, with detailed results provided in the supplementary (Suppl. File 1) [27]. Furthermore, Bayesian ANCOVA and linear regression tests were performed to investigate the results, which showed an insignificant effect for one of the dose groups, and these findings were also added to the supplementary file (Suppl. File 1).

Data were expressed as mean ± standard deviation (SD) for animal behavioral tests, and graphs were generated using GraphPad Prism (version 9.0). Statistical analysis for behavioral tests was performed using two-way repeated measures analysis of variance (ANOVA) for all time points, utilizing SPSS software (version 15, SPSS Inc., Chicago, USA). Additionally, one-way ANOVA followed by the least significant difference (LSD) test was employed to compare groups on the days of behavioral experiments, with statistical significance set at $p < 0.05$. Random Coefficients Models were constructed to investigate the effect of time and dose on behavioral markers, and the time*dose interaction was tested using SAS® Version 9.4 (Cary, North Carolina, USA). Furthermore, a two-way ANOVA was applied to explore the interaction between neuronal survival, injured neurons, intact neurons, and DNA fragmentation. To describe the association between brain cortical atrophy and distance traveled in the open field test, the Spearman rank correlation coefficient was computed using SPSS (version 15, SPSS Inc., Chicago, USA). LC–MS/MS data were evaluated using independent samples t-tests, with a 1.4-fold change considered significant between vehicle and 5 mg/kg or 10 mg/kg VPN-treated groups.

Results

After Cold-Induced TBI, VPN Reduces Infarct Volume, Brain Swelling, and BBB Disruption

Firstly, we analyzed whether the vehicle or VPN treatments affected mice's body weights after cold-induced TBI. The results showed that there was no difference in the body weights of mice before TBI and after 28 days of low or high doses of VPN treatment (Suppl. Fig. S1). To observe the effect of VPN on infarct volume and brain swelling, animals were sacrificed 48 h after cold-induced TBI. Results demonstrated that low-dose (5 mg/kg) or high-dose (10 mg/kg) VPN significantly reduced infarct volume in the acute phase (48 h after TBI) of cold-induced TBI (Fig. 2A). Low-dose VPN slightly but high dose of VPN significantly decreased the brain swelling (Fig. 2B). We also assessed BBB disruption using Evans blue dye extravasation, which does not typically cross the BBB under physiological conditions due to its high molecular weight (961 Da) and its binding to the large protein molecule albumin, which also does not usually cross the BBB [28]. Results showed that VPN treatment significantly preserved the BBB integrity in a dose-dependent manner (Fig. 2C).

High Dose of VPN (10 mg/kg) Decreased Cold-Induced TBI-Induced Disseminated Neuronal Injury

A cold-induced TBI causes neuronal loss and DNA fragmentation in the injured area. Brain sections from bregma were stained with NeuN, and NeuN + cells in both injured and non-injured cortex were counted to evaluate neuronal survival. Both doses of VPN slightly but not significantly increased neuronal survival ($p = 0.076$ for high-dose VPN) after cold-induced TBI (Fig. 3A). Cresyl violet staining was conducted to observe the differences in the numbers of injured and non-injured (intact) neurons following VPN administration (Fig. 3 B and C). It was observed that 10 mg/kg VPN significantly reduced the number of injured neurons in the ipsilesional cortex but did not affect the number of intact neurons. To explore the impact of VPN intake on disseminated neuronal injury, we conducted a TUNEL assay. Our findings revealed that while low-dose VPN had a slight effect, high-dose VPN significantly reduced the number of DNA fragmented cells in the injured area (Fig. 3D).

The interaction between neuronal survival, injured neurons, intact neurons, and DNA fragmentation was also investigated (Suppl. Figure 2). Based on the results, analyses with a similar dose–response relationship in the same direction were grouped together. No significant interaction effect was observed for neuronal survival and intact neurons; however, both dose and variant were significant predictors of the response. Similarly, no significant interaction effect or variable influence was found for injured neurons and DNA fragmentation, although a significant dose effect was identified.

Daily VPN Treatment Increases Locomotor Activity and Reduces Brain Atrophy After Cold-Induced TBI

This study also investigated the effects of long-term VPN administration after cold-induced TBI. For this purpose, low-dose or high-dose VPN administration started 48 h after cold-induced TBI and continued for 26 days. Spontaneous locomotor activity, anxiety-like behavior, and exploration behavior were assessed using an open-field test. Overall locomotor activity was reduced on the second day after cold-induced TBI. Compared to the vehicle, low-dose VPN slightly and high-dose VPN significantly increased the traveled distance in the open field test at 2, 7, and 28 days post-cold-induced TBI (Fig. 4A). Additionally, the high dose of VPN increased mobility time and decreased immobility time, indicating increased spontaneous locomotor activity (Fig. 4B–C). VPN also increased the time spent in the core (center) zone (Fig. 4D) and transition zone (Fig. 4E) while decreasing the time spent in the open field wall (outer) zone (Fig. 4F), suggesting a partial reversal of the anxious phenotype induced by TBI.

Moreover, exploration behavior was analyzed by the number of transitions between zones. Both doses of VPN treatment increased exploration behavior in mice after TBI (Suppl. Figure 3A–D). The percent change of each behavioral marker from baseline to follow-up time points (2, 7, 14, and 28 days after dosing initiation) was calculated. We tested for time effect, dose effect, and their interaction. No significant time*dose interactions were found, so these interaction terms were removed. In the reduced models, no time effect was observed on any of the six markers, suggesting that behavioral markers did not change significantly over time. However, the dose effect was significant for distance, mobility, transition, and wall zone, particularly between the 10 mg/kg dose and the vehicle (Suppl. File 2 and Suppl. Fig. S4). The response difference between the vehicle and 5 mg/kg VPN was 17.76 ($p = 0.02$), while the difference between the vehicle and 10 mg/kg VPN was 30.08 ($p < 0.0001$), both of which were statistically significant. For mobility time, the response difference between the vehicle and 5 mg/kg VPN was 5.67, but this difference was not statistically significant ($p = 0.44$). In contrast, the response difference between the vehicle and 10 mg/kg VPN was 19.26, which was statistically significant ($p = 0.01$). For the transition marker, there was no significant difference between the vehicle and 5 mg/

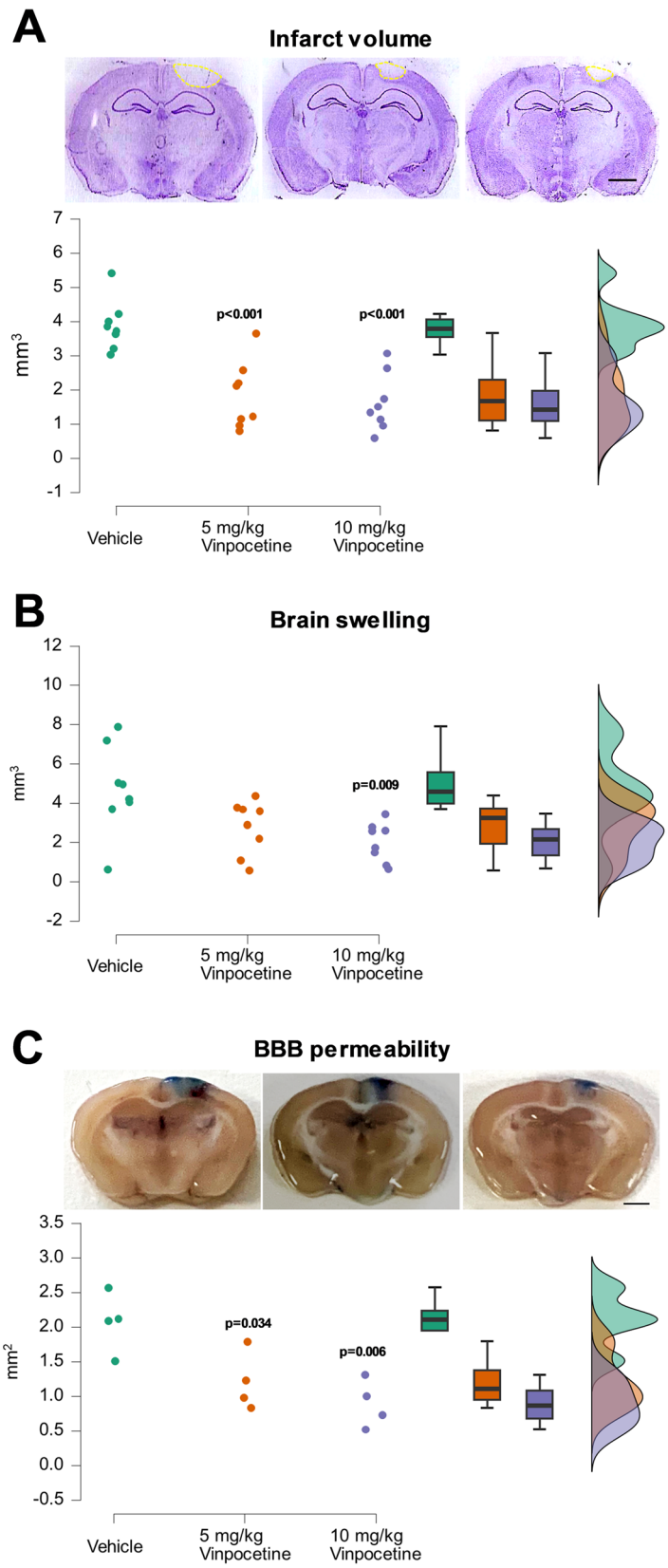

Fig. 2 Effect of VPN on infarct volume (**A**), brain swelling (**B**), and BBB disruption (**C**) after cold-induced TBI. Infarct volume and brain swelling were evaluated using cresyl violet stained sections ($n=8$ mice/group). Note that 5 mg/kg or 10 mg/kg VPN treatment significantly reduced brain infarct volume. In addition, 10 mg/kg VPN decreased brain swelling and BBB permeability compared to the vehicle and 5 mg/kg VPN group ($n=4$ mice/group). The data is depicted through raincloud plots featuring jittering alongside visual representations of the median, IQR boxes, and 95% CI for each quantitative attribute. Scale bars are 1 mm

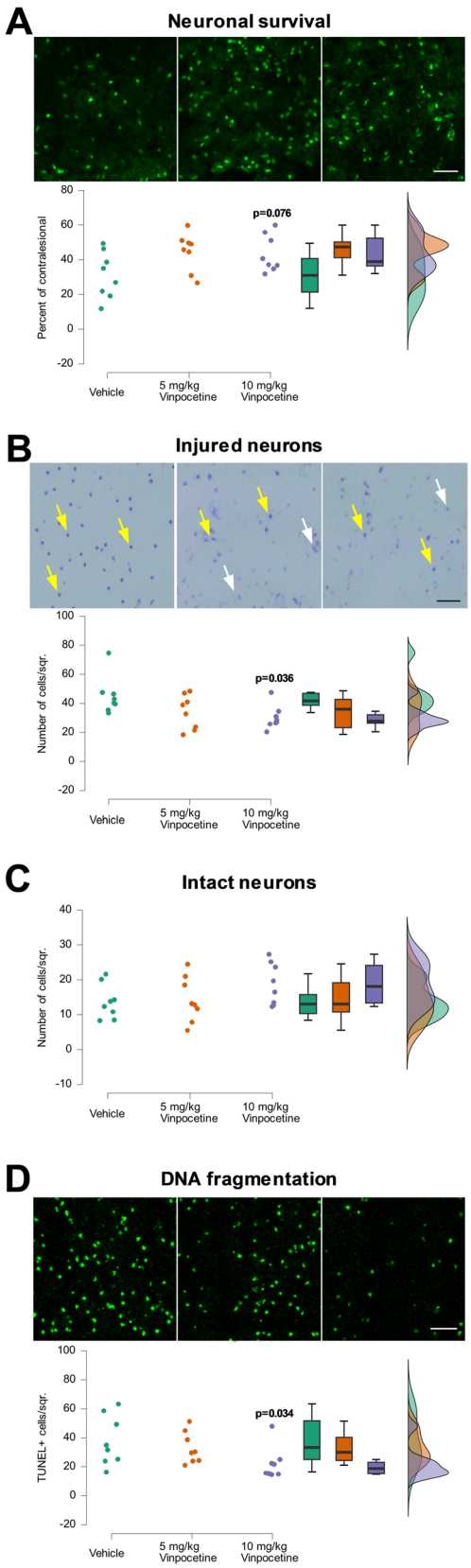

Fig. 3 VPN decreased disseminated neuronal injury. VPN slightly but not significantly increased neuronal survival after cold-induced TBI, which was evaluated by NeuN staining (**A**). Injured (**B**) and intact (**C**) neurons were evaluated from cresyl violet stained sections. The yellow arrows indicate injured neurons, while the white arrows indicate intact neurons. Note that high dose of VPN decreased injured neurons but did not affect the number of intact neurons. In addition, high dose of VPN decreased the DNA fragmentation evaluated by TUNEL staining (**D**). The data is depicted through raincloud plots featuring jittering alongside visual representations of the median, IQR boxes, and 95% CI for each quantitative attribute ($n=8$ mice/group). Scale bars are 50 µm

kg VPN ($p=0.84$), with a response of 2.60, whereas the response to the 10 mg/kg VPN dose was 58.47, with a significant difference ($p<0.0001$). The wall-zone showed no significant difference, with a response of 7.57 ($p=0.17$) for the vehicle and 5 mg/kg, and − 11.50 ($p=0.04$) with a significant difference for the vehicle and 10 mg/kg VPN. The core zone showed no significant differences for either dose: − 12.52 with a p value of 0.66 (5 mg/kg) and 33.35 with a p value of 0.25 (10 mg/kg). Similarly, immobility showed significant differences for both doses: − 9.00 with a p value of 0.67 (5 mg/kg) and 0.90 with a p value of 0.97 (10 mg/kg).

The long-term impact of cold-induced TBI causes brain atrophy in the injured cortex, which controls movement. To evaluate brain atrophy, cresyl violet staining was performed on coronal sections obtained from long-term cold-induced TBI experiments (Fig. 5A). Notably, a high dose of VPN treatment reduced whole-brain atrophy (Fig. 5B) and motor cortex atrophy (Fig. 5C). However, VPN intake did not affect sensory cortex atrophy (Fig. 5D). Additionally, a significant inverse correlation was observed between brain cortical atrophy and the distance traveled in the open field test. This suggests that as cortical atrophy increases, locomotor activity in mice decreases. Mobility also decreased as cortical atrophy increased (Suppl. Fig. S5).

Daily VPN Administration Dose-Dependently Increases Neurogenesis After Cold-Induced TBI

To observe the effect of VPN on newly formed cells and neurogenesis in the injured cortex, immunohistochemistry was performed using antibodies against BrdU (used as a cell proliferation marker) and NeuN (used as a neuronal marker). VPN increased the number of newly formed cells in a dose-dependent manner (Fig. 6A). Similarly, the co-expression of BrdU and NeuN which is related to neurogenesis slightly increased dose-dependently after cold-induced TBI (Fig. 6B). To investigate the effects of VPN on neuronal migration and differentiation processes, we analyzed the number of cells co-expressing BrdU and doublecortin (DCX), used as a marker for migrating neurons. The results indicated no differences between the groups. Furthermore,

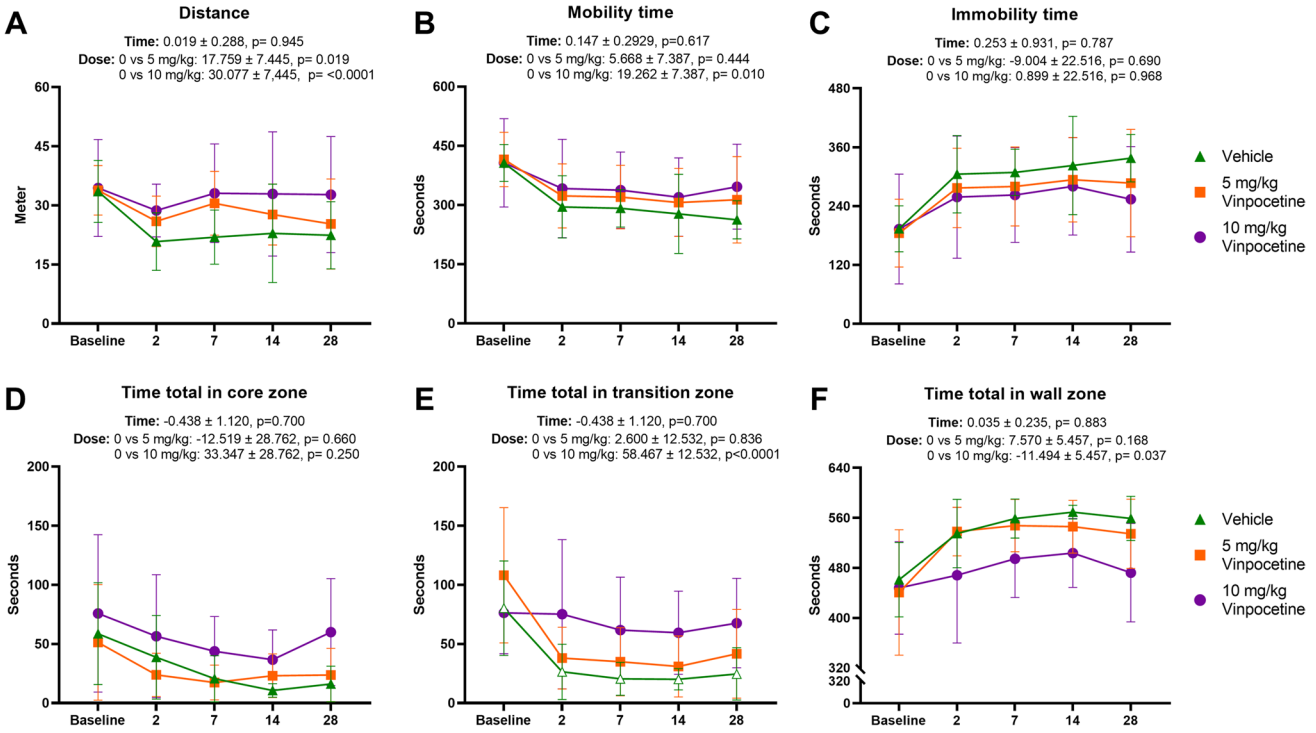

Fig. 4 High dose of VPN (10 mg/kg/day) increased spontaneous locomotor activity after cold-induced TBI. The open-field test was performed to examine the effect of VPN on spontaneous locomotor activity and anxiety-like behavior. Results demonstrated that only high dose of VPN increased traveled distance (**A**), mobility time (**B**), and decreased immobility time (**C**) in open field test associated with spontaneous locomotor activity, besides total time in core zone (**D**), transition zone (**E**) increased, and time total in wall zone (**F**) decreased for both VPN dose. Data are represented as mean ± SD values ($n = 12$ mice/ group)

the percentage of newly formed NeuN-positive or DCX-positive cells was analyzed (Suppl. Fig. S6A–B). However, no difference in percentage was found between the groups.

Identification of VPN-Regulated Proteins via *LC–MS/MS*

Injured cortex tissues were analyzed by liquid chromatography-tandem mass spectrometry (LC–MS/MS) to identify the differentially regulated proteins after VPN treatment. A total of 1317 proteins were identified in the vehicle and VPN-treated groups. Our analyses revealed that 192 proteins for ipsilesional cortex tissue (Fig. 7A) exhibited statistically significant variations ($p < 0.05$ and 1.4-fold change). To comprehensively assess the proteome profile within the injured cortex, we plotted log2 fold changes against the t-test derived negative log 10 p-values for all differentially regulated proteins in vehicle or VPN-treated groups (Suppl. Fig. S6). Subsequently, we applied a threshold using a > 1.4-fold change in conjunction with the − log (p-value) > 1.4 criterion. Results demonstrated that expressions of 84 proteins were reduced, and 108 proteins were elevated in ipsilesional tissue (Fig. 7A). In addition, pathway analysis was conducted using the Protein ANalysis THrough Evolutionary Relationships (PANTHER) classification system (Fig. 7B) and the Database for Annotation, Visualization, and Integrated Discovery (DAVID) (v2023q4, https://david.ncifcrf.gov/) to utilize KEGG, REACTOME, and WikiPathways databases (Suppl. Fig. S8 and Suppl. Fig. S9).

According to the PANTHER analysis, the top-scored pathways were Huntington's disease (clathrin light chain B (CLTB), dynein light chain 2 (DYNLL2), glutamate receptor ionotropic, NMDA 2B (GRIN2B), Ras-related C3 botulinum toxin substrate 1 (RAC1), Rho-related GTP-binding protein RhoG (RHOG), synaptojanin-1 (SYNJ), tubulin beta-1 chain (TUBB1), and tubulin beta-6 chain (TUBB6)), Parkinson's disease (casein kinase II subunit alpha (CSNK2A1), NADH dehydrogenase [ubiquinone] flavoprotein 2 (NDUFV), proteasome subunit alpha type-1 (PSMA1), proteasome subunit alpha type-5 (PSMA5), Septin-4 (SEPTIN4), and 14–3-3 protein zeta/delta (YWHAZ)), Wnt signaling pathway (CSNK2A1, C-terminal-binding protein 1 (CTBP1), guanine nucleotide-binding protein G(I)/G(S)/G(O) subunit gamma-7 (GNG7), myosin-6 (MYH6), calcineurin subunit B type 1 (PPP3R1), and protein kinase C epsilon type (PRKCE)), inflammation mediated by chemokine and cytokine signaling pathway (GNG7, MYH6, RAC1, PRKCE, and RHOG), integrin signaling pathway (collagen

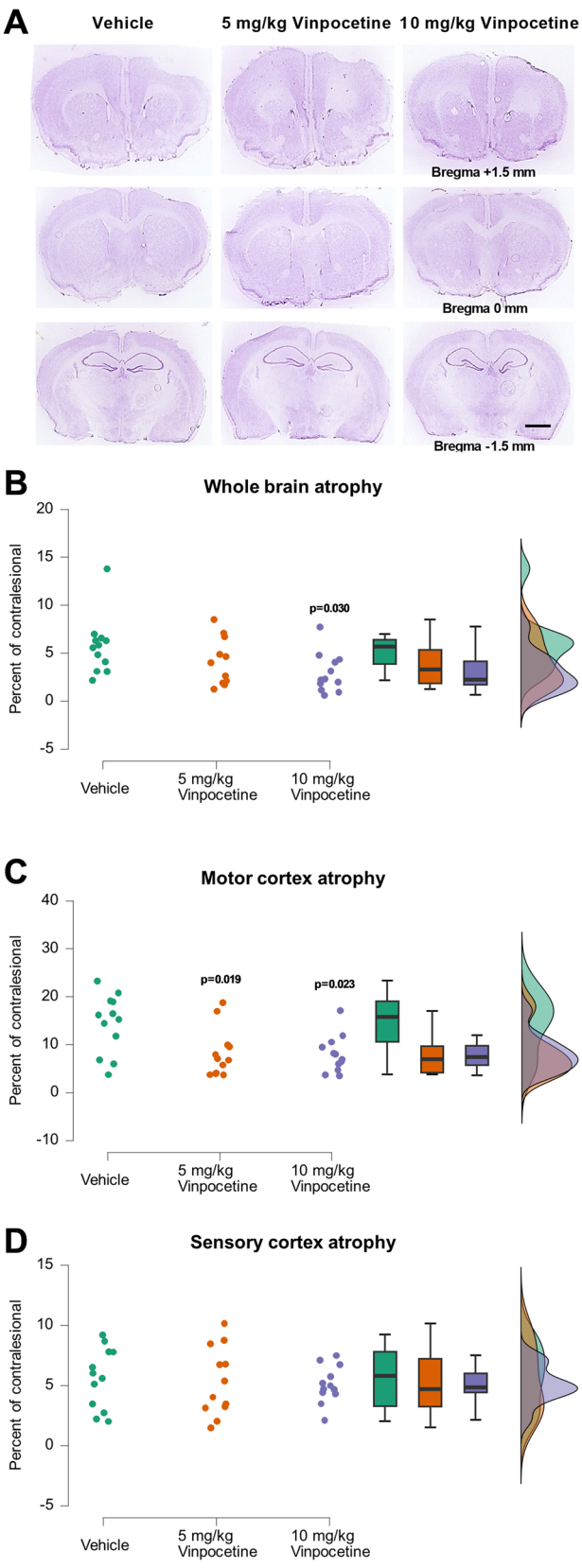

Fig. 5 Long-term VPN administration reduces brain atrophy after cold-induced TBI. To analyze brain atrophy, sections from equidistant brain levels, 1 mm apart, were stained with cresyl violet in mice sacrificed 28 days post-TBI (**A**). A high dose of VPN (10 mg/kg/day) decreased whole brain atrophy (**B**) and motor cortex atrophy (**C**) but did not affect sensory cortex atrophy. The data are depicted through raincloud plots featuring jittering alongside visual representations of the median, IQR boxes, and 95% CI for each quantitative attribute ($n = 12$ mice/group). Scale bar: 1 mm

type V alpha 3 chain (COL5A3), RAC1, vinculin (VCL), and talin-1 (TLN1)), ionotropic glutamate receptor pathway (GRIN2B, metabotropic glutamate receptor 3 (GRM3), SH3 and multiple ankyrin repeat domains protein 1 (SHANK1), and SH3 and multiple ankyrin repeat domains protein 3 (SHANK3)), cytoskeletal regulation by Rho GTPase (MYH6, RAC1, TUBB1, and TUBB6), EGF receptor signaling pathway (PRKCE, RAC1, RHOG, and YWHAZ), and ubiquitin proteasome pathway (26S proteasome regulatory subunit 7 (PSMC2), 26S proteasome non-ATPase regulatory subunit 3 (PSMD3), 26S proteasome non-ATPase regulatory subunit 11 (PSMD11), and ubiquitin-like modifier-activating enzyme 6 (UBA6)).

The DAVID analysis identified 24 pathways from KEGG, 151 pathways from REACTOME, and 5 pathways from WikiPathways (Suppl. Fig. S8, Suppl. Fig. S9, and Suppl. Fig. S10). The top-scored pathways were visualized as enrichment bubble plots (Fig. 8A–C). In the top 10 results of the KEGG pathway analysis (Fig. 8A), prion disease exhibited a high enrichment value with the lowest p value. The disease-related core KEGG pathways with high scores mainly include ubiquinol-cytochrome c reductase, complex III subunit X (Uqcr10), Rac family small GTPase 1 (Rac1), calmodulin 1 (Calm1), cytochrome c oxidase subunit 7A2 (Cox7a2), NADH/ubiquinone oxidoreductase core subunit S8 (Ndufs8), NADH/ubiquinone oxidoreductase core subunit V2 (Ndufv2), NADH/ ubiquinone oxidoreductase subunit A10 (Ndufa10), NADH/ubiquinone oxidoreductase subunit B1 (Ndufb1), and NADH/ubiquinone oxidoreductase subunit B3 (Ndufb3). In the top 10 results of the REACTOME pathway analysis (Fig. 8B), protein–protein interactions at synapses showed the lowest p value. In contrast, the synaptic adhesion-like molecules pathway exhibited the highest enrichment value. For the core REACTOME pathways, it is observed as mostly common proteins, which are dynein light chain LC8-type 2 (Dynll2), protein phosphatase 3, regulatory subunit B, alpha isoform (calcineurin B, type I) (Ppp3r1), discs large MAGUK scaffold protein 2 (Dlg2), calmodulin 1 (Calm1), spectrin beta, non-erythrocytic 1 (Sptbn1), spectrin beta, non-erythrocytic 2 (Sptbn2), and ankyrin 1, erythroid (Ank1). Also, Rac1 gene was observed mainly at the high score results of PANTHER. Other affected pathways included beta-catenin independent WNT signaling, signaling by WNT, regulation of mRNA stability

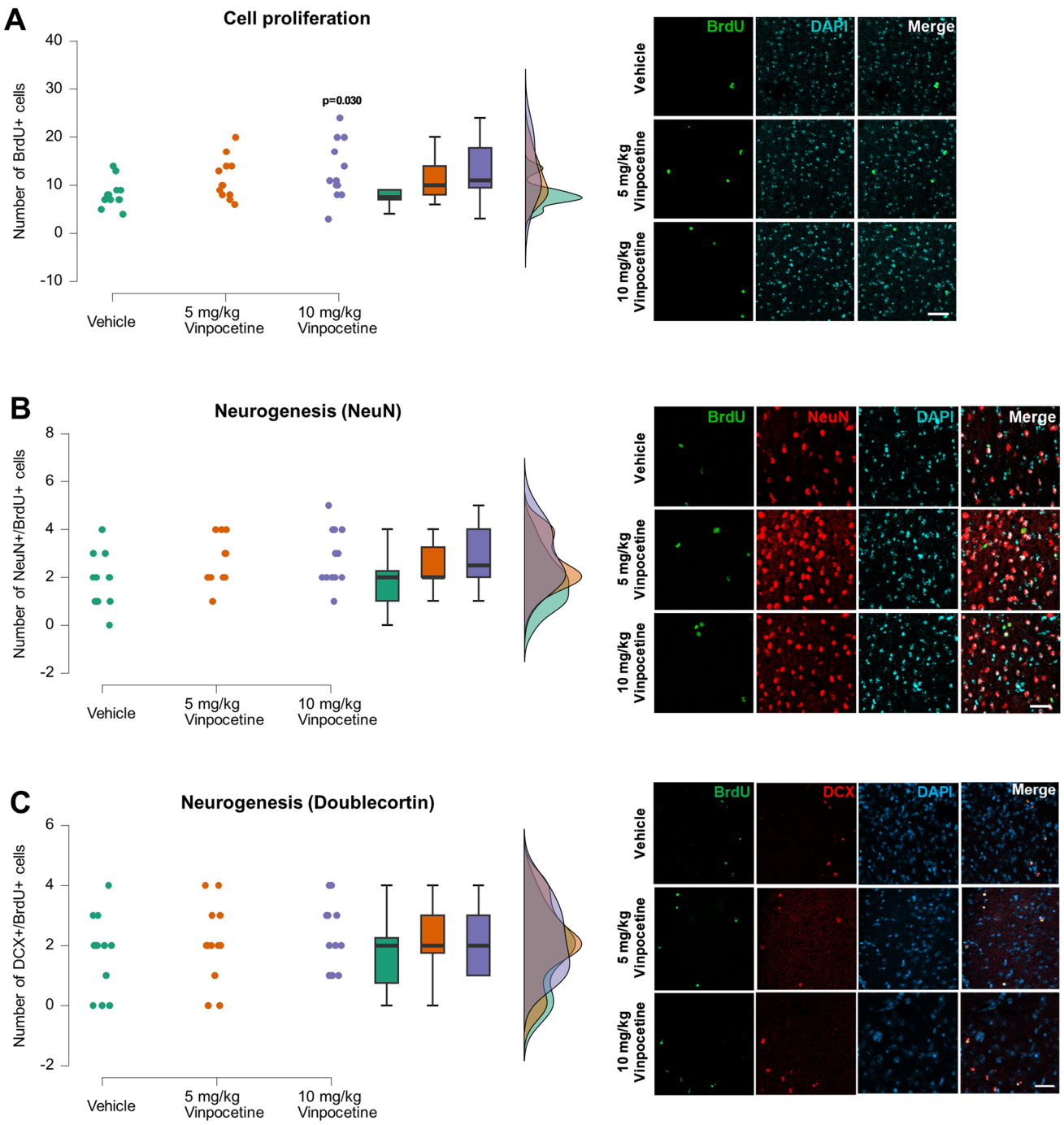

Fig. 6 A high dose of VPN significantly increases cell proliferation, and slightly increases neurogenesis after TBI. To examine cell proliferation and differentiation, 100 mg/kg BrdU was administered via intraperitoneal injection every 3 days, starting 48 h after the onset of cold-induced TBI. Cell proliferation was determined by BrdU incorporation analysis in animals sacrificed 28 days post-TBI (**A**). Newly formed neurons were assessed by the co-expression of NeuN and BrdU (**B**) or DCX and BrdU (**C**) incorporating cells. The data are depicted through raincloud plots featuring jittering alongside visual representations of the median, IQR boxes, and 95% CI for each quantitative attribute ($n = 12$ mice/group). Scale bars are 50 µm

by proteins that bind AU-rich elements, separation of sister chromatids, L1CAM interactions, neuronal system, programmed cell death, and the citric acid (TCA) cycle, and respiratory electron transport pathways. The WikiPathways analysis revealed pathways such as the electron transport chain, glycogen metabolism, splicing factor NOVA-regulated synaptic proteins, translation factors, and proteasome degradation pathways (Fig. 8C). Supplementary Information

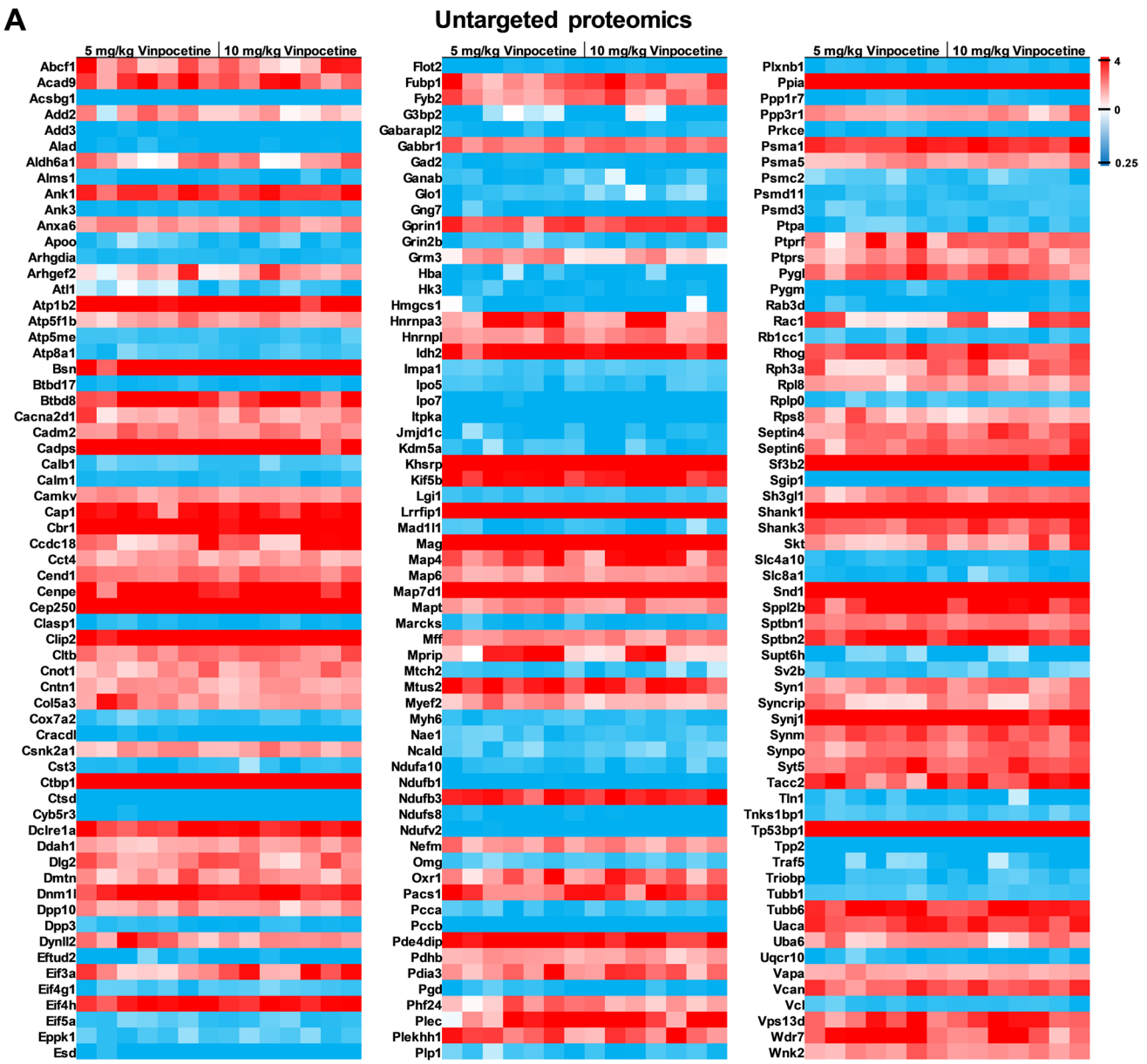

Fig. 7 Identification of the protein profile affected by VPN by liquid chromatography-tandem mass spectrometry (LC–MS/MS) in the injured area at 28 days post-cold-induced TBI. A total of 192 protein expressions were altered ($p < 0.05$ and fold change > 1.4) depending on VPN treatment. The results are shown as a heat map (**A**). Moreover, differentially abundant proteins due to VPN administration were classified by Protein ANalysis THrough Evolutionary Relationships (PANTHER, http://pantherdb.org) pathway analysis (**B**) ($n = 7$ mice/group)

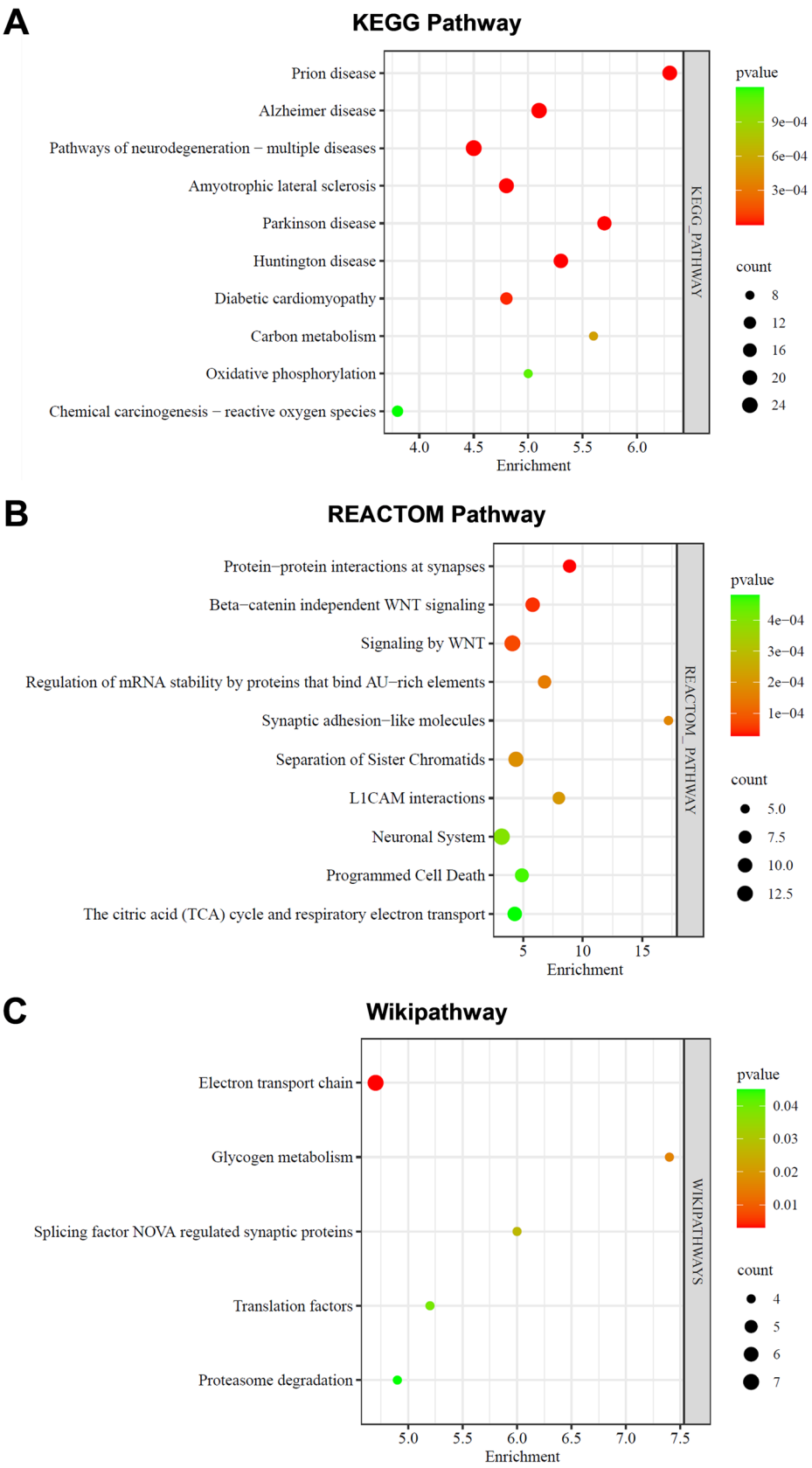

Fig. 8 Pathway analysis of differentially expressed proteins (DEPs) affected by VPN. A total of 192 DEPs were clustered based on the Kyoto Encyclopedia of Genes and Genomes (KEGG) (**A**), REACTOM (**B**), and WikiPathways (**C**)

(Suppl. File 1 and Suppl. File 3) provides a detailed list of the affected proteins included in these pathways.

Discussion

VPN demonstrates a range of therapeutic benefits and emerges as a promising therapeutic candidate for various neurological disorders. Studies highlight its efficacy in improving conditions such as stroke, traumatic brain injury, dementia, Parkinson's disease (PD), and epilepsy [10, 29, 30]. VPN modulates neurotransmitter pathways and neuronal activity, reducing seizure frequency and enhancing cognitive functions. Its ability to regulate calcium and sodium levels in brain cells contributes to its neuroprotective function, offering potential avenues for intervention in conditions characterized by neuronal damage or dysfunction [31, 32]. Notably, VPN's anti-inflammatory, antioxidant, and antiapoptotic properties hold promise for the treatment of neurological disorders where oxidative stress and neuroinflammation play significant roles in disease progression [4]. Moreover, studies show that VPN alleviates the oxidative stress caused by cold-induced TBI, restores brain neurochemicals, and improves motor functions post-injury. The observed neuroprotective effects of VPN may stem from its antioxidant potential and have the ability to restore brain neurochemicals under stress conditions [3]. By enhancing the phosphorylation of cAMP response element-binding protein (p-CREB), VPN facilitates critical signaling pathways involved in neuronal plasticity and memory formation. This mechanism offers a potential target for therapeutic interventions aimed at ameliorating cognitive impairments associated with brain injury [33, 34]. However, there is currently limited literature on the use of VPN specifically in the context of cold-induced TBI, highlighting the need for further research to elucidate its efficacy and mechanisms in this area.

In the current study, we investigated the effect of VPN on cold-induced TBI in mice with a low dose (5 mg/kg) or high dose (10 mg/kg). Previously, Hou and colleagues demonstrated that administering 10 mg/kg of VPN reduced brain infarct volume and apoptosis following transient middle cerebral artery occlusion-induced cerebral ischemia in mice [35]. Based on these and similar studies, a dose range was established in accordance with the literature. We found that both low-dose and high-dose VPN significantly reduced infarct volume and brain swelling in the acute phase of cold-induced TBI, with the high dose showing a more pronounced effect. Additionally, VPN preserved BBB integrity dose-dependently, as evidenced by reduced Evans blue dye extravasation. These findings are consistent with existing literature that highlights VPN's neuroprotective properties. Other studies have shown that VPN improves cerebral metabolism by increasing glucose and oxygen supply and ATP production through cerebral vasodilation. It achieves this by enhancing the levels of neurotransmitters such as serotonin, dopamine, and noradrenaline, which are crucial for cognitive function, thereby helping to prevent ischemia-induced memory and cognitive dysfunctions. In addition, Wang et al. showed that VPN inhibits Nf-κB protein expression and prevents pro-inflammatory cytokine formation after the ischemia/reperfusion model, thus preventing the development of brain swelling [33]. This role should contribute to its neuroprotective actions after cold-induced TBI, highlighting the neuroprotective effect of VPN and supporting findings from other studies [36]. Corroborating our findings, Bereczki and Fekete demonstrated that VPN reduced the size of cerebral infarction after middle cerebral artery occlusion in animal models. Moreover, VPN has been shown to increase cerebral perfusion and oxygen extraction in controlled human studies, preventing the worsening of attention in patients with multiple cerebral infarcts [1].

The present study demonstrates that VPN intake significantly enhances neuronal survival, which NeuN staining evaluated following cold-induced TBI in mice. Therefore, we assessed the disseminated neuronal injury using the TUNEL assay. Notably, our results demonstrate a dose-dependent effect, with 10 mg/kg of VPN exhibiting more pronounced reductions in DNA fragmented cells within the ipsilesional tissue compared to 5 mg/kg treatment. This indicates that higher doses of VPN are more effective in mitigating neuronal damage post-TBI. Additionally, we utilized cresyl violet staining to distinguish between intact and injured neurons after VPN intake. We observed that VPN intake increased the number of intact neurons while decreasing the number of injured neurons. In addition to these findings, we explored the relationship between VPN and neurogenesis through NeuN, BrdU, and doublecortin immunohistochemical staining. The results showed a slight, dose-dependent increase in neurogenesis with VPN treatment. This suggests that VPN may play a role in enhancing the brain's regenerative capacity following TBI.

Our results demonstrated that a daily intake of 10 mg/kg VPN was associated with increased locomotor activity and decreased anxiety-like behavior in the mice. Additionally, our observation of reduced brain atrophy in the motor cortex following VPN treatment supports these findings. The significant correlation between reduced brain atrophy and increased locomotor activity observed in our study, as assessed by the open field test, underscores the interplay between structural and functional recovery mechanisms in neurodegenerative conditions affecting motor functions. Furthermore, our results align with those of Kajal Bagri and Rahul Deshmukh, who demonstrated that VPN restores cognitive and motor functions in rats challenged with traumatic brain injury [3]. This reinforces the potential of VPN

to enhance cognitive and motor recovery post-TBI, highlighting its promise as a therapeutic agent in such contexts.

Our study's large-scale proteomic analysis provides novel insights into the mechanisms of VPN and its therapeutic potential in TBI, shedding light on previously unexplored protein targets and pathways that may underlie its neuroprotective effects. In the current study, for the first time, a large-scale proteomic analysis was performed to determine affected proteins by VPN treatment in the injured brain tissue using LC–MS/MS. Thus, we identified 192 differentially abundant proteins in the vehicle and VPN-treated groups. VPN treatment decreased the expression of 84 and increased the expression of 108 of these proteins. In the injured tissue, the expression of peptidyl-prolyl cis–trans isomerase A (Ppia), sodium/potassium-transporting ATPase subunit beta-2 (Atp1b2), and spectrin beta chain, non-erythrocytic 1 (Sptbn1), were most abundantly increased, and the expressions of inositol-trisphosphate 3-kinase A (Itpka), myosin-6 (Myh6), and leucine-rich glioma-inactivated protein 1 (Lgi1) were most abundantly decreased. Ppia, also known as cyclophilin A, regulates protein folding, trafficking, assembly, immune modulation, and cell signaling [37]. Sptbn1 is a cytoskeletal protein involved in various cellular functions, including apoptosis, cell cycle regulation, adhesion, and synaptogenesis [38]. Itpka, associated with the inositol signaling pathway, has many roles in cognitive functions, calcium signal transduction, brain development, and stress responses [39]. Dysfunction in the protein expression is involved in immune system diseases, neurodegenerative disorders, and cancer [40]. In addition, VPN treatment increased Myh6, which is essential for cell migration, intracellular transport, secretion, and synaptogenesis, and Lgi1, which is important for glutamatergic synapses and regulates neuronal excitability [41, 42].

The findings presented provide essential insights into VPN's therapeutic potential in TBI by elucidating its impact on protein expression levels and pathways involved in neuroprotection and repair processes. Inhibiting the RhoA-ROCK signaling pathway emerges as a promising therapeutic strategy for CNS disorders, including TBI, by preserving neural connectivity and preventing cell death. Traumatic activation of integrins and subsequent involvement of the Rho pathway in diffuse axonal injury highlight the importance of exploring integrin-mediated mechanisms in TBI pathology for targeted therapeutic interventions [43]. Additionally, addressing extracellular glutamate levels and ionotropic glutamate receptor-mediated excitotoxicity post-TBI presents potential therapeutic targets for improving neuronal survival and function [44]. Furthermore, exploring protein ubiquitination's role in axonal integrity preservation and the dysregulation of pathways in vascular- and trauma-induced brain injuries underscore their relevance as targets for innovative therapeutic interventions post-injury [45]. Preserving mitochondrial function, understanding alterations in neuronal surface interactions, and investigating the role of the L1 cell adhesion molecule in TBI hold promise for improving outcomes [46–48]. Additionally, the significant accumulation of glycogen post-TBI suggests a potential protective mechanism worth exploring further [49]. Acute impacts on synaptic long-term plasticity, protein degradation pathways, and neuroinflammatory pathways underscore the need for deeper understanding and precise therapeutic interventions to optimize patient outcomes while minimizing complications associated with neuroinflammation [50, 51]. In summary, our findings underscore VPN's potential as a promising therapeutic candidate for traumatic brain injury, highlighting its neuroprotective effects and suggesting avenues for further research to optimize its clinical application and efficacy in improving patient outcomes.

It is important to acknowledge several limitations when interpreting this study's findings. The repetitive use of the open field test may diminish its predictive power over time due to animal habituation effects. Additionally, since there was no sham group in the study, the effect of VPN in physiological conditions was not shown. These limitations must be considered when interpreting the study's findings to ensure their reliability and validity. Despite these insights, future studies incorporating a sham group and longitudinal assessments could further validate VPN's efficacy and elucidate its long-term effects, thereby enhancing the reliability and clinical applicability of our findings.

Conclusion

In conclusion, this study demonstrated how low-dose (5 mg/kg) and high-dose (10 mg/kg) VPN affect infarct volume, brain swelling, and BBB integrity in cold-induced TBI. Additionally, we observed VPN's anti-apoptotic properties and its impact on the brain's motor area. Moreover, our findings suggest that VPN slightly increases neurogenesis and may have a curative effect on cold-induced TBI, expanding on previous data related to other neurological conditions.

Supplementary Information The online version contains supplementary material available at https://doi.org/10.1007/s12035-024-04515-8.

Author Contribution This work was carried out in collaboration between all authors. HEY, SBB, and SA conducted the animal experiments and analyzed the data. HIK and SB carried out the behavioral tests. HEY and ZD performed the immunofluorescence and LC–MS/MS experiments and analyzed the data. HEY, MK, and MCB performed statistical analyses throughout the manuscript. NO, MK, EK, and MCB defined the research theme and revised the manuscript critically.

Funding This work was supported by The Scientific and Technological Research Council of Turkey (TUBITAK; 218S453, to MCB), Turkish Academy of Sciences (TUBA; to EK).

Data Availability The datasets analyzed during the current study are openly available.

Declarations

Ethics Approval This study has been conducted under the ethics standards of the EU Guidelines on the Care and Use of Laboratory Animals (Directive 2010/63/EU) in agreement with local guidelines and legislation and has been approved by the Animal Research Ethics Committee of Istanbul Medipol University (reference number: 10/01/2022–05).

Consent of Participate Not applicable.

Consent for Publication Not applicable.

Conflict of interest The authors declare competing interests.

References

1. Al-Kuraishy H, Al-Gareeb A, Naji M, Al-Mamorry F (2020) Role of vinpocetine in ischemic stroke and poststroke outcomes: a critical review. Brain Circ 6:1. https://doi.org/10.4103/bc.bc_46_19
2. Deshmukh R, Sharma V, Mehan S et al (2009) Amelioration of intracerebroventricular streptozotocin induced cognitive dysfunction and oxidative stress by vinpocetine - a PDE1 inhibitor. Eur J Pharmacol 620:49–56. https://doi.org/10.1016/j.ejphar.2009.08.027
3. Bagri K, Deshmukh R (2022) Vinpocetine restores cognitive and motor functions in traumatic brain injury challenged rats. Inflammopharmacology 30:2243–2259. https://doi.org/10.1007/s10787-022-01059-y
4. Al-kuraishy HM, Alexiou A, Papadakis M et al (2023) New insights on the potential effect of vinpocetine in Parkinson's disease: one of the neglected warden and baffling topics. Metab Brain Dis 38:1831–1840. https://doi.org/10.1007/s11011-023-01254-y
5. Delhaye S, Bardoni B (2021) Role of phosphodiesterases in the pathophysiology of neurodevelopmental disorders. Mol Psychiatry 26:4570–4582. https://doi.org/10.1038/s41380-020-00997-9
6. Medina AE (2011) Therapeutic utility of phosphodiesterase type I inhibitors in neurological conditions. Front Neurosci 5:2007–2011. https://doi.org/10.3389/fnins.2011.00021
7. Svab G, Doczi J, Gerencser AA et al (2019) The mitochondrial targets of neuroprotective drug vinpocetine on primary neuron cultures, brain capillary endothelial cells, synaptosomes, and brain mitochondria. Neurochem Res 44:2435–2447. https://doi.org/10.1007/s11064-019-02871-9
8. O'Brien JJ, O'Callaghan JP, Miller DB et al (2020) Inhibition of calcium-calmodulin-dependent phosphodiesterase (PDE1) suppresses inflammatory responses. Mol Cell Neurosci 102:103449. https://doi.org/10.1016/j.mcn.2019.103449
9. Gómez CD, Buijs RM, Sitges M (2014) The anti-seizure drugs vinpocetine and carbamazepine, but not valproic acid, reduce inflammatory IL-1β and TNF-α expression in rat hippocampus. J Neurochem 130:770–779. https://doi.org/10.1111/jnc.12784
10. Zhao M, Hou S, Feng L et al (2020) Vinpocetine protects against cerebral ischemia-reperfusion injury by targeting astrocytic Connexin43 via the PI3K/AKT signaling pathway. Front Neurosci 14:1–14. https://doi.org/10.3389/fnins.2020.00223
11. Patyar S, Prakash A, Modi M, Medhi B (2011) Role of vinpocetine in cerebrovascular diseases. Pharmacol Reports 63:618–628. https://doi.org/10.1016/S1734-1140(11)70574-6
12. Ping Z, Xiaomu W, Xufang X, Liang S (2019) Vinpocetine regulates levels of circulating TLRs in Parkinson's disease patients. Neurol Sci 40:113–120. https://doi.org/10.1007/s10072-018-3592-y
13. Samidurai A, Xi L, Das A et al (2021) Role of phosphodiesterase 1 in the pathophysiology of diseases and potential therapeutic opportunities. Pharmacol Ther 226:107858. https://doi.org/10.1016/j.pharmthera.2021.107858
14. Zhou B, Lin W, Long Y et al (2022) Notch signaling pathway: architecture, disease, and therapeutics. Signal Transduct Target Ther 7:1–33. https://doi.org/10.1038/s41392-022-00934-y
15. Hayat R, Manzoor M, Hussain A (2022) Wnt signaling pathway: a comprehensive review. Cell Biol Int 46:863–877. https://doi.org/10.1002/cbin.11797
16. Ahmad N, Lesa KN, Sudarmanto A et al (2022) The role of phosphodiesterase-1 and its natural product inhibitors in Alzheimer's disease: a review. Front Pharmacol 13:1–16. https://doi.org/10.3389/fphar.2022.1070677
17. Han P, Werber J, Surana M et al (1999) The calcium/calmodulin-dependent phosphodiesterase PDE1C down-regulates glucose-induced insulin secretion. J Biol Chem 274:22337–22344. https://doi.org/10.1074/jbc.274.32.22337
18. Maas AIR, Menon DK, Manley GT et al (2022) Traumatic brain injury: progress and challenges in prevention, clinical care, and research. Lancet Neurol 21(11):1004–1060. https://doi.org/10.1016/S1474-4422(22)00309-X
19. Ciftci E, Karacay R, Caglayan A et al (2020) Neuroprotective effect of lithium in cold- induced traumatic brain injury in mice. Behav Brain Res 392:112719. https://doi.org/10.1016/j.bbr.2020.112719
20. Kelestemur T, Yulug B, Caglayan AB et al (2016) Targeting different pathophysiological events after traumatic brain injury in mice: role of melatonin and memantine. Neurosci Lett 612:92–97. https://doi.org/10.1016/j.neulet.2015.11.043
21. Kilic E, Reitmeir R, Kilic Ü et al (2014) HMG-CoA reductase inhibition promotes neurological recovery, peri-lesional tissue remodeling, and contralesional pyramidal tract plasticity after focal cerebral ischemia. Front Cell Neurosci 8:1–10. https://doi.org/10.3389/fncel.2014.00422
22 Beker MC, Caglayan AB, Kelestemur T et al (2015) Effects of normobaric oxygen and melatonin on reperfusion injury: role of cerebral microcirculation. Oncotarget 6:30604–30614. https://doi.org/10.18632/oncotarget.5773
23. Beker MC, Caglayan B, Yalcin E et al (2018) Time-of-day dependent neuronal injury after ischemic stroke: implication of circadian clock transcriptional factor Bmal1 and survival kinase AKT. Mol Neurobiol 55:2565–2576. https://doi.org/10.1007/s12035-017-0524-4
24. Tang D, Chen M, Huang X et al (2023) SRplot: a free online platform for data visualization and graphing. PLoS ONE 18:1–8. https://doi.org/10.1371/journal.pone.0294236
25 Allen M, Poggiali D, Whitaker K et al (2019) Raincloud plots: a multi-platform tool for robust data visualization. Wellcome Open Res 4:1–52. https://doi.org/10.12688/wellcomeopenres.15191.1
26. Clément MA, Bosoi CR, Oliveira MM et al (2021) Bile-duct ligation renders the brain susceptible to hypotension-induced neuronal degeneration: implications of ammonia. J Neurochem 157:561–573. https://doi.org/10.1111/jnc.15290
27. Peter Rosenfeld J, Olson JM (2021) Bayesian data analysis: a fresh approach to power issues and null hypothesis interpretation. Appl Psychophysiol Biofeedback 46:135–140. https://doi.org/10.1007/s10484-020-09502-y
28. de Goldim MP, S, Della Giustina A, Petronilho F, (2019) Using Evans blue dye to determine blood-brain barrier integrity in

rodents. Curr Protoc Immunol 126:1–7. https://doi.org/10.1002/cpim.83
29. Gjerulfsen CE, Mieszczanek TS, Johannesen KM et al (2023) Vinpocetine improved neuropsychiatric and epileptic outcomes in a patient with a GABRA1 loss-of-function variant. Ann Clin Transl Neurol 10:1493–1498. https://doi.org/10.1002/acn3.51838
30. Ishola IO, Awogbindin IO, Olubodun-Obadun TG et al (2023) Vinpocetine prevents rotenone-induced Parkinson disease motor and non-motor symptoms through attenuation of oxidative stress, neuroinflammation and α-synuclein expressions in rats. Neurotoxicology 96:37–52. https://doi.org/10.1016/j.neuro.2023.03.002
31. Erro R, Mencacci NE, Bhatia KP (2021) The emerging role of phosphodiesterases in movement disorders. Mov Disord 36:2225–2243. https://doi.org/10.1002/mds.28686
32. Sitges M, Galván E, Nekrassov V (2005) Vinpocetine blockade of sodium channels inhibits the rise in sodium and calcium induced by 4-aminopyridine in synaptosomes. Neurochem Int 46:533–540. https://doi.org/10.1016/j.neuint.2005.02.001
33. Wang H, Zhang K, Zhao L et al (2014) Anti-inflammatory effects of vinpocetine on the functional expression of nuclear factor-kappa B and tumor necrosis factor-alpha in a rat model of cerebral ischemia-reperfusion injury. Neurosci Lett 566:247–251. https://doi.org/10.1016/j.neulet.2014.02.045
34. Krahe TE, Wang W, Medina AE (2009) Phosphodiesterase inhibition increases CREB phosphorylation and restores orientation selectivity in a model of fetal alcohol spectrum disorders. PLoS One 4:e6643. https://doi.org/10.1371/journal.pone.0006643
35. Hou B, Li D, Wang D et al (2023) Neuroprotective effects of vinpocetine against ischemia-reperfusion injury via inhibiting NLRP3 inflammasome signaling pathway. Neuroscience 526:74–84. https://doi.org/10.1016/j.neuroscience.2023.05.021
36. Dong ZC, Shi Y, Liu LJ et al (2024) Synthesis and pharmacological activity of vinpocetine derivatives. RSC Adv 14:7981–7991. https://doi.org/10.1039/d3ra07325d
37. Nigro P, Pompilio G, Capogrossi MC (2013) Cyclophilin A: a key player for human disease. Cell Death Dis 4:1–10. https://doi.org/10.1038/cddis.2013.410
38. Yang P, Yang Y, Sun P et al (2020) βII spectrin (SPTBN1): Biological function and clinical potential in cancer and other diseases. Int J Biol Sci 17:32–49. https://doi.org/10.7150/ijbs.52375
39. Xia HJ, Yang G (2005) Inositol 1,4,5-trisphosphate 3-kinases: functions and regulations-trisphosphate 3-kinase (IP 3 3-kinase/IP3K), inositol polyphosphate kinase (Ipk), inositol phos-phate multikinase (Ipmk), calcium (Ca 2+), signal transduction. Cell Res 15:83–91
40. Chung S, Kim IH, Lee D et al (2016) The role of inositol 1,4,5-trisphosphate 3-kinase A in regulating emotional behavior and amygdala function. Sci Rep 6:1–10. https://doi.org/10.1038/srep23757
41. Kornau HC, Kreye J, Stumpf A et al (2020) Human cerebrospinal fluid monoclonal LGI1 autoantibodies increase neuronal excitability. Ann Neurol 87:405–418. https://doi.org/10.1002/ana.25666
42. Osterweil E, Wells DG, Mooseker MS (2005) A role for myosin VI in postsynaptic structure and glutamate receptor endocytosis. J Cell Biol 168:329–338. https://doi.org/10.1083/jcb.200410091
43. Mulherkar S, Tolias KF (2020) RhoA-ROCK signaling as a therapeutic target in traumatic brain injury. Cells 9:1–13. https://doi.org/10.3390/cells9010245
44. Baracaldo-Santamaría D, Ariza-Salamanca DF, Corrales-Hernández MG et al (2022) Revisiting excitotoxicity in traumatic brain injury: from bench to bedside. Pharmaceutics 14:1–26. https://doi.org/10.3390/pharmaceutics14010152
45. Staal JA, Dickson TC, Chung RS, Vickers JC (2009) Disruption of the ubiquitin proteasome system following axonal stretch injury accelerates progression to secondary axotomy. J Neurotrauma 26:781–788. https://doi.org/10.1089/neu.2008.0669
46. Palzur E, Edelman D, Sakas R, Soustiel JF (2021) Etifoxine restores mitochondrial oxidative phosphorylation and improves cognitive recovery following traumatic brain injury. Int J Mol Sci 22:12881. https://doi.org/10.3390/ijms222312881
47. Park K, Biederer T (2013) Neuronal adhesion and synapse organization in recovery after brain injury. Future Neurol 8:555–567. https://doi.org/10.2217/fnl.13.35
48. Jiang H, Giarratana AO, Theis T et al (2024) Single nucleotide polymorphism in cell adhesion molecule L1 affects learning and memory in a mouse model of traumatic brain injury. Int J Mol Sci 25:3043. https://doi.org/10.3390/ijms25053043
49. Otori T, Friedland JC, Sinson G et al (2004) Traumatic brain injury elevates glycogen and induces tolerance to ischemia in rat brain. J Neurotrauma 21:707–718. https://doi.org/10.1089/089771504126962 3
50. Feldmann LK, Le PF, Felzen V et al (2019) Proteasome and autophagy-mediated impairment of late long-term potentiation (L-ltp) after traumatic brain injury in the somatosensory cortex of mice. Int J Mol Sci 20:1–17. https://doi.org/10.3390/ijms20123048
51. Di Battista AP, Rhind SG, Hutchison MG et al (2016) Inflammatory cytokine and chemokine profiles are associated with patient outcome and the hyperadrenergic state following acute brain injury. J Neuroinflammation 13:1–14. https://doi.org/10.1186/s12974-016-0500-3